Supplementary Information (SI) for Lab on a Chip.

Supplementary Materials for

Microfluidic Sperm Trap Array for Single-Cell Flagellar Analysis with Unrestricted Flagellar Movement

Kaiyu Wang *et al.*

Corresponding author: Junhua Yuan, jhyuan@ustc.edu.cn; Rongjing Zhang, rjzhang@ustc.edu.cn

This PDF file includes:

Other Supplementary Materials for this manuscript include the following:

Movies S1 to S6

Evaluation of the sperm activity in a sealed glass-PDMS-glass chamber over one hour

We evaluated whether sperm in the device can maintain their activity during the observation period (~1 hour), considering factors such as nutrient depletion, metabolite accumulation (due to the lack of medium refreshment), and potential water evaporation and CO_2 leakage (as the thin PDMS layer in the chamber remains gas-permeable). To assess sperm activity retention, we measured several Computer-Aided Sperm Analysis (CASA) parameters of freely swimming sperm in the device before and after a one-hour interval. These parameters include curvilinear velocity (VCL, time-averaged velocity of a sperm head along its actual curvilinear path), average path velocity (VAP, velocity over an average path generated by a roaming average), straight-line velocity (VSL, the time-averaged velocity of the sperm head along a straight line from its first position to its last position), wobble (WOB, defined as VAP/VCL), and linearity (LIN, defined as VSL/VAP). These parameter values before and after (mean $\pm$ standard deviation) the one-hour period are as follows: 120.51 $\pm$ 37.87 *vs.* 121.51 $\pm$ 38.60 (VCL), 95.21 $\pm$ 39.97 *vs.* 91.94 $\pm$ 37.82 (VAP), 76.05 $\pm$ 44.58 *vs.* 74.17 $\pm$ 41.02 (VSL), 0.7680 $\pm$ 0.1824 *vs.* 0.7376 $\pm$ 0.1771 (WOB), 0.7450 $\pm$ 0.2460 *vs.* 0.7557 $\pm$ 0.2334 (LIN). These parameters did not change significantly during the one-hour period, indicating that the sperm in the device maintain stable conditions even without medium refreshment over this duration.

Clarifying the apparent contradiction of hyperactivation agents' impact on flagellar beating harmonics

Our results indicate that as the concentration of 4-AP increases, there is a significant increase in the asymmetric component of flagellar curvature. This is evidenced by increases in both the fundamental (C_0) and the second ($|C_2\sin\Phi|$) asymmetric harmonic intensities. However, these effects manifest differently along the flagellum: C_0 shows a significant increase only within the segment $s \in [5, 20]$ μm, whereas $|C_2\sin\Phi|$ exhibits a significant increase across the entire length of the flagellum. Notably, only at $s > 20$ μm does $|C_2\sin\Phi|$ contribute significantly to the change in flagellar asymmetry.

Two different studies have reported changes in one of these two parameters (C_0 or $|C_2\sin\Phi|$) under the stimulation of hyperactivation agents, but did not detect changes in the other parameter—the

one observed by the other study.[1, 2] At first glance, their findings appear to conflict with each other and with our own. However, we propose that this perceived discrepancy is due to variations in the measurement sites along the flagellum. Through comprehensive analysis across the entire flagellum, as performed in our study, such misunderstandings can be resolved.

One study by G. Saggiorato et al. induced hyperactivation in human sperm using progesterone and observed a significant increase in $|C_2\sin\Phi|$.[1] Their measurements were taken at s = 15 and 25 μm along the sperm flagellum, coinciding with the relative range in bovine sperm flagellum where we noted a substantial contribution of $|C_2\sin\Phi|$ to the asymmetry change (both located at the principal piece). This overlap in measurement regions may suggest a subtle evolutionary conservation of flagellar mechanics between human and bovine sperm. However, these positions do not align with the segment where we detected a significant change in C_0, hence they did not detect a notable change in C_0.

Conversely, M. Zaferani et al. examined the effect of 4-AP on bovine sperm flagellar behavior, finding that 4-AP induced an increase in C_0 alone from a baseline of zero, without any detectable $|C_2\sin\Phi|$ signal, regardless of the presence or absence of 4-AP stimulation.[2] Their measurements were focused around s = 10 μm, where our findings indicate that the change in C_0 is pronounced, facilitating its detection. In contrast, the change in $|C_2\sin\Phi|$ is much smaller than that of C_0 in this region, making it less noticeable. This could be the reason they only detected C_0 without the signal of $|C_2\sin\Phi|$. Additionally, their study mainly focused on the hyperactivation effect on sperm boundary-following behavior, thus mainly requiring the observation of swimming sperm rather than sperm flagella. They employed a relatively low frame rate (25 or 50 fps), which may have been sufficient for their primary focus but insufficient to capture the subtle $|C_2\sin\Phi|$ signal amid the high-frequency flagellar beating.

In summary, the discrepancies between these studies can be attributed to the different measurement positions on the flagellum, highlighting the importance of comprehensive analysis across the entire flagellum. A notable advantage of our device is its ability to ensure the free beating of the entire flagellum without structural constraints. This capability allows for a complete analysis across the flagellum, thus enhancing the authenticity, comprehensiveness, and reliability of our conclusions.

Analytical calculation of power dissipation

The flagellar beating amplitude in *x* and *y* directions can be written as:

$$x = x_1 \sin(ks - 2\pi ft) + x_2 \sin(ks - 4\pi ft + \phi_x), \tag{S1}$$

$$y = y_1 \sin(ks - 2\pi ft) + y_2 \sin\big(ks - 4\pi ft + \phi_y\big), \tag{S2}$$

$$k = \frac{2\pi}{L}. \tag{S3}$$

Therefore the beating velocities in *x* and *y* directions are:

$$v_x = -2\pi f x_1 \cos(ks - 2\pi ft) - 4\pi f x_2 \cos(ks - 4\pi ft + \phi_x), \tag{S4}$$

$$v_y = -2\pi f y_1 \cos(ks - 2\pi ft) - 4\pi f y_2 \cos(ks - 4\pi ft + \phi_y). \tag{S5}$$

The force applied to surrounding fluid by a flagellum unit was calculated utilizing resistive-force theory[3]:

$$\vec{F} = \xi_t\big(\vec{v} \cdot \vec{t}\big)\vec{t} + \xi_n(\vec{v} \cdot \vec{n})\vec{n} \tag{S6}$$

where $\vec{t}$ and $\vec{n}$ denote the flagellum's tangent and normal vectors, and ξ_t and ξ_n are the tangent and normal friction coefficients, respectively. We use the capitalization *F* to distinguish it from the flagellar beat frequency *f*. The power dissipation of a flagellum unit *p* (denoted as power dissipation density hereafter) is:

$$p = \vec{F} \cdot \vec{v} = F_t v_t + F_n v_n = \xi_t v_t^2 + \xi_n v_n^2, \tag{S7}$$

where v_t and v_n are the tangent and normal component of the velocity $\vec{v}$, respectively. Considering the anisotropic drag coefficient's relationship $\xi_n \approx 2\xi_t$ for a slender body as the flagellum, Eq. S7 becomes:

$$p = \xi_t(v^2 + v_n^2) \tag{S8}$$

with the contribution term of v_n^2 originating from the drag anisotropy. The flagellum possesses a certain degree of flexibility, resulting in a variation in the ratio of v_n^2 and v^2 along the flagellum, with high values (close to 1) at the anterior and low values (close to 0) at the posterior area (see Fig. S9 for $\frac{v_n^2}{v^2}$'s dependence on the *s* position). We simply captured this tendency utilizing a linear falling function $\left(1 - \frac{s}{L}\right)$ and obtained:

$$p = \xi_t v^2 \left(2 - \frac{s}{L}\right) = \xi_t\big(v_x^2 + v_y^2\big)\left(2 - \frac{s}{L}\right). \tag{S9}$$

Considering the magnitudes in Eqs. S4-5 and substituting them into Eq. S9, we obtained an expression of time-averaged power dissipation density:

$$\bar{p} = f\int_0^{\frac{1}{f}} dt\, p = \varepsilon\mu f^2[(x_1^2 + 4x_2^2 + 4x_1x_2) + (y_1^2 + 4y_2^2 + 4y_1y_2)]\left(2 - \frac{s}{L}\right). \quad \text{(S10)}$$

Here, μ denotes the fluid dynamic viscosity, which, coupled with flagellar geometry, linearly determines the value of ξ_t, and ξ_n;[4] ε is a dimensionless proportional coefficient that comes from the time integration and the ratio of ξ_t and μ. Note that the effect of friction between the flagellum and the PDMS/glass surfaces was automatically incorporated into ξ_t and ξ_n.

We explored the analytical expressions of y_1, y_2, x_1, and x_2 by proper fittings. We first fitted the shapes of y_1 and x_1 using cosine-based functions:

$$y_1 \text{ or } x_1 = a \cdot \cos[b(s - c)] + d, \quad \text{(S11)}$$

obtaining reasonable fitting results across all conditions (see Figs. S6-7). We then fitted y_2 and x_2 based on the shapes of y_1 and x_1, respectively, by multiplying by a ratio factor:

$$y_2 = \alpha y_1, \quad \text{(S12)}$$

$$x_2 = \beta x_1, \quad \text{(S13)}$$

since we observed an approximately proportional relationship between the first and second-harmonic amplitude (see Figs. S6-7). Substituting these fitting parameters from Eqs. S11-13 into Eq. S10, we obtained:

$$\bar{p} = \varepsilon\mu f^2\left(g_\beta x_1^2 + g_\alpha y_1^2\right)\left(2 - \frac{s}{L}\right), \quad \text{(S14)}$$

where g_α and g_β are functions of α and β, respectively, sharing the same form:

$$g_\alpha = 1 + 4\alpha^2 + 4\alpha \quad \text{(S15)}$$

$$g_\beta = 1 + 4\beta^2 + 4\beta \quad \text{(S16)}$$

Finally, we obtained the expression for the time-averaged power dissipation of the entire flagellum by integrating Eq. S14 along the flagellum (*s*-axis):

$$\bar{P} = \varepsilon\mu f^2\left(g_\beta X_1 + g_\alpha Y_1\right), \quad \text{(S17)}$$

where X_1 and Y_1 represent the integration of $\left(2 - \frac{s}{L}\right)x_1^2$ and $\left(2 - \frac{s}{L}\right)y_1^2$ along the *s*-axis, respectively. The X_1 and Y_1 share the same form:

$$\{8L^2b^2d^2s + a[2Lb(a(2bL - \sin(2bc - 2bL)) + a\sin(2bc) + 8d\sin(bc) - 8d\sin(bc - bL)) + a(-b^2L^2 + bL\sin(2bc - 2bL) + \sin(bc - bL)^2) - a\sin(bc)^2 + 8bdL\sin(bc - bL) + 8d\cos(bc) - 8d\cos(bc - bL)] - 2b^2d^2L\}/4Lb^2 \quad \text{(S18)}$$

We also provide a MATLAB code for the same expression of Eq. S18:

```
(a*(8*d*cos(b*c) + a*(sin(b*(c - L))^2 - b^2*L^2 + b*L*sin(2*b*(c - L))) - 8*d*cos(b*(c - L)) - a*sin(b*c)^2 - 2*L*b*(a*(sin(2*b*(c - L)) - 2*b*L) - a*sin(2*b*c) - 8*d*sin(b*c) + 8*d*sin(b*(c - L))) + 8*b*d*L*sin(b*(c - L))) - 2*b^2*d^2*L^2 + 8*L^2*b^2*d^2)/(4*L*b^2).
```

Numerical calculation of power dissipation

We utilized Eqs. S6 and S7 with time-averaged integration to numerically calculate the time-averaged power dissipation density. Further integrating along the flagellum yields the total flagellar power dissipation. The transverse and normal drag coefficients, ξ_t and ξ_n, were calculated similarly to a previous study[5]:

$$\xi_t = \frac{2\pi\mu}{ln(\frac{2q}{a})}, \quad \text{(S19)}$$

and

$$\xi_n = \frac{4\pi\mu}{ln(\frac{2q}{a})+\frac{1}{2}}, \quad \text{(S20)}$$

where the viscosity $\mu = 0.001$ Pa s; q is a characteristic scale length, a small fraction of the wavelength L ($L = 44$ μm, $q = 0.09L = 3.6$ μm); and a denotes the radius of the flagellum (taken as 0.5 μm). We also adopted the same values in the corresponding analytical calculations, if used.

Adaptation of the trapping structure for human and murine sperm

The geometry, size, and motility behavior of human sperm are relatively similar to those of bovine sperm, which we primarily used in our current studies. Therefore, only minor adjustments are necessary to adapt our trapping structure for human sperm. Specifically, the width and length of the head trapping groove can be slightly reduced to better fit the dimensions of the human sperm head, ensuring effective capture.

In contrast, murine sperm poses a greater challenge due to significant differences in morphology, size, and motility behavior compared to bovine sperm. Murine sperm heads are typically sickle-shaped and smaller in size. Adapting our device for murine sperm would require a more substantial redesign of the head trapping structure, involving reshaping the groove to match the curved head of murine sperm and adjusting its dimensions to accommodate the smaller size. Additionally, because the flagellum of murine sperm is longer and its movement more asymmetric than that of bovine sperm, the trap slot must be widened both horizontally and vertically to prevent the flagellum from extending out or contacting the sidewalls.

While this theoretical approach shows promise, further research is required to refine and optimize this concept to ensure its practical effectiveness in capturing sperm from species other than bovine.

Supplementary references

1. G. Saggiorato, L. Alvarez, J. F. Jikeli, U. Benjamin Kaupp, G. Gompper and J. Elgeti, *Nat. Commun.*, 2017, **8**, 1415.
2. M. Zaferani, S. S. Suarez and A. Abbaspourrad, *Proc. Natl. Acad. Sci. U.S.A.*, 2021, **118**, e2107500118.
3. J. Gray and G. J. Hancock, *J. Exp. Biol.*, 1955, **32**, 802-814.
4. R. E. Johnson and C. J. Brokaw, *Biophys. J.*, 1979, **25**, 113-127.
5. E. H. Ooi, D. J. Smith, H. Gadêlha, E. A. Gaffney and J. Kirkman-Brown, *R. Soc. open sci.*, 2014, **1**, 140230.

Supplementary Figures

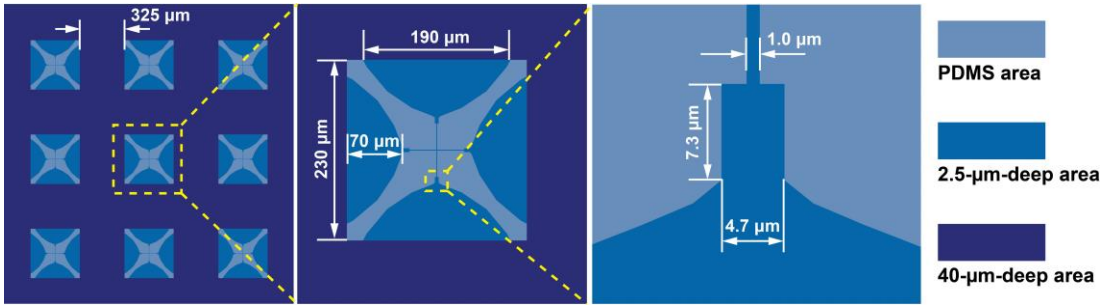

Fig. S1. Critical dimensions of the trap structures.

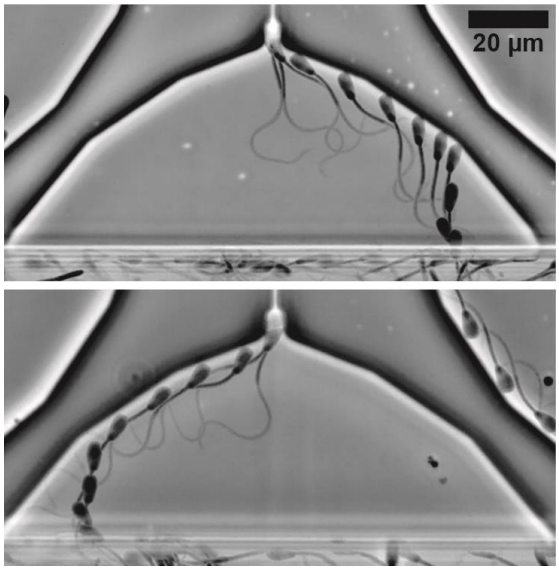

Fig. S2. Overlapping snapshots of two additional examples showing sperm yawing towards the trap slot sidewall, ultimately leading to their entrapment through the two-dimensional boundary-following mechanism.

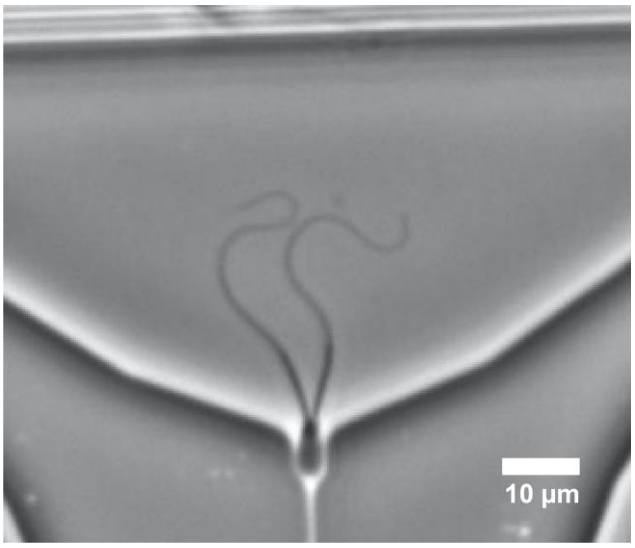

Fig. S3. An example of a multiple-sperm group consisting of two sperm squeezed into a single groove.

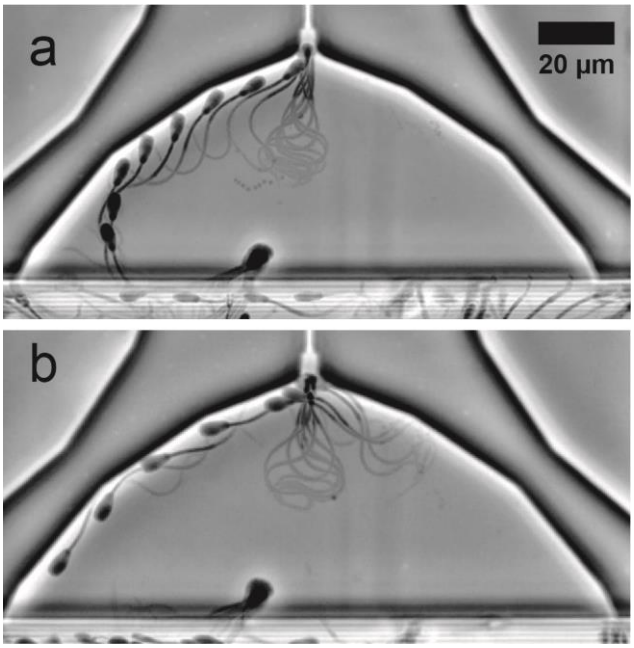

Fig. S4. Overlapping snapshots for a case of an unsuccessful attempt to organize two sperm into a trap groove (also shown in Movie S4). (a) One sperm advances towards the trap groove already occupied by another sperm, attempting to squeeze in. (b) Due to the limited space in the groove, which is partially occupied by the preceding sperm, and the repulsive force generated by its flagellum beat, the subsequent sperm fails to enter and swims away.

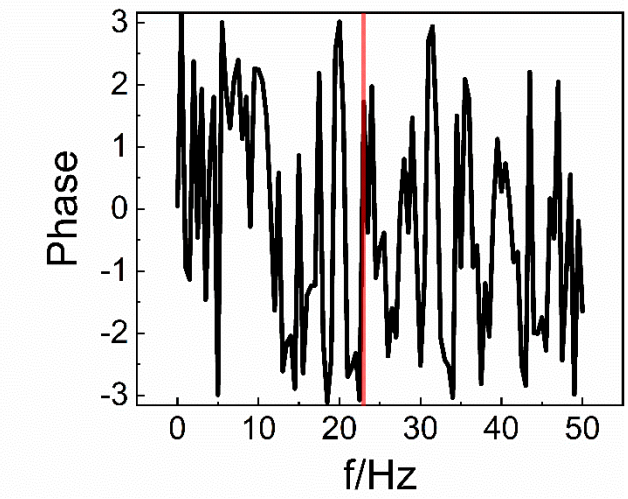

Fig. S5. The curvature phase spectrum from the same Fourier analysis as Fig. 3B. The red vertical line denotes the position of the second-harmonic peak in the corresponding amplitude spectrum, as shown in Fig. 3B. The phase value at this position was used to calculate the second-harmonic intensity parameter, as discussed in the main text.

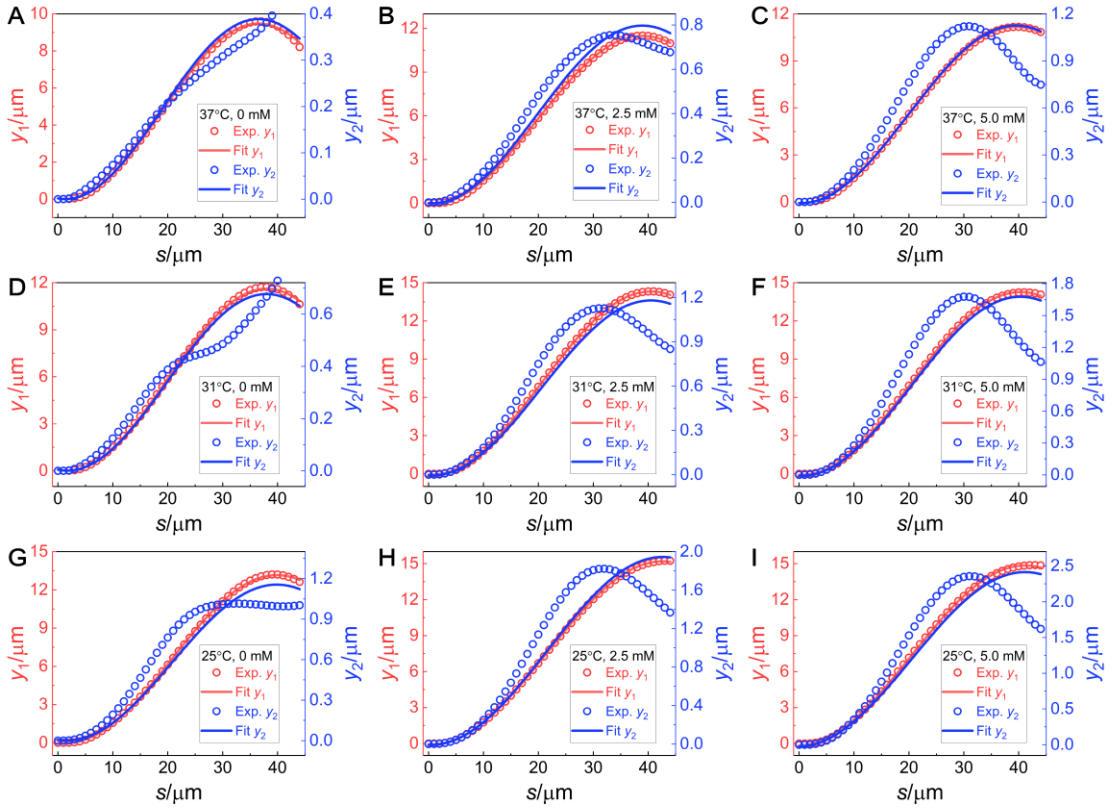

Fig. S6. Fitting results for y_1 and y_2 under each temperature and 4-AP concentration condition (37°C, 31°C, and 25°C; 0 mM, 2.5 mM, and 5.0 mM 4-AP). y_1 and y_2 are plotted together for each condition, with y_1 corresponding to the left axis (denoted in red) and y_2 to the right axis (denoted in blue).

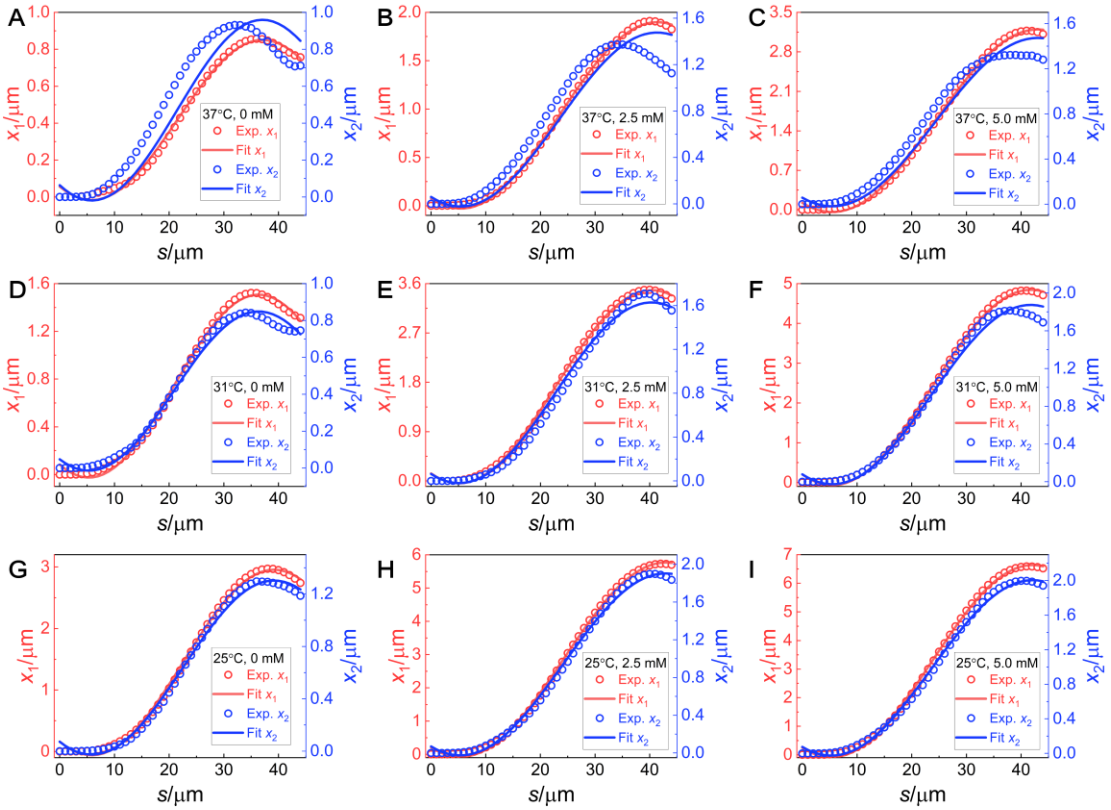

Fig. S7. Fitting results for x_1 and x_2 under each temperature and 4-AP concentration condition (37°C, 31°C, and 25°C; 0 mM, 2.5 mM, and 5.0 mM 4-AP). x_1 and x_2 are plotted together for each condition, with x_1 corresponding to the left axis (denoted in red) and x_2 to the right axis (denoted in blue).

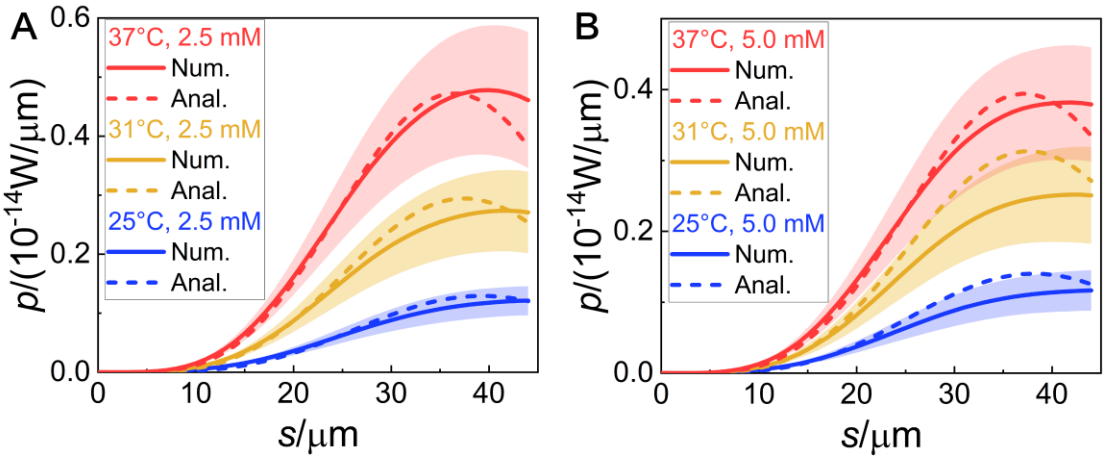

Fig. S8. Comparison of numerical and analytical calculations of flagellar power density under various temperature and 4-AP concentration conditions. A. 2.5 mM 4-AP at 37℃, 31℃, and 25℃. B. 5.0 mM 4-AP at 37℃, 31℃, and 25℃.

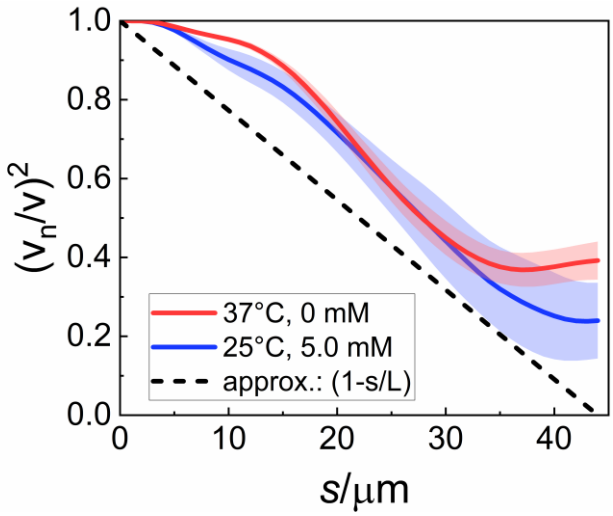

Fig. S9. Variation of $\frac{v_n^2}{v^2}$ along the flagellum under two extreme conditions (37°C with 0 mM 4-AP and 25°C with 5.0 mM 4-AP). The dashed line denotes our linear approximation of the $\frac{v_n^2}{v^2}$ trend.

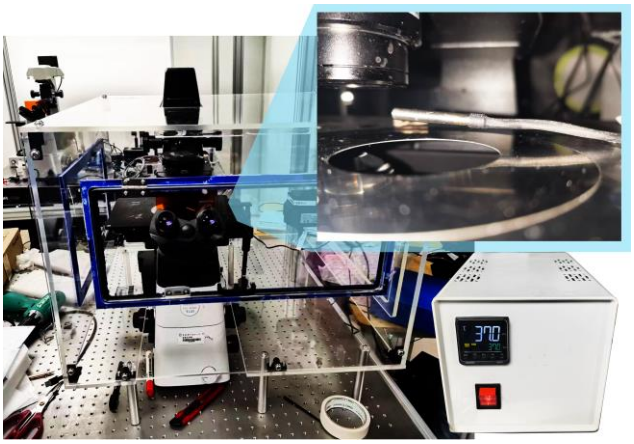

Fig. S10. Photos of the constant temperature enclosure system. The inset shows a close-up of the microscope stage's sample port, with the temperature probe positioned nearby to ensure accurate sample temperature measurements.

Supplementary Videos

Movie S1. An example showing typical cases of success and failure in sperm capture, with one sperm crossing the groove without being captured and another becoming trapped in the groove.

Movie S2. Slow-motion footage (at one-tenth the original speed) of a trapped sperm.

Movie S3. The most extreme case of hyperactivated sperm behavior induced by 4-aminopyridine (4-AP) at a concentration of 5.0 mM and a temperature of 25 degrees Celsius, resulting in vigorous flagellar beating (shown in slow motion at one-tenth the original speed).

Movie S4. A case of an unsuccessful attempt to organize multiple sperm into the trap groove, as shown in Fig. S4.

Movie S5. An example of a sperm trapped and exhibiting hyperactivated behavior at a 4-AP concentration of 5.0 mM and a temperature of 37 degrees Celsius.

Movie S6. An example of a sperm trapped at 25 degrees Celsius without 4-AP stimulation, displaying behavior similar to that under a hyperactivated state (as seen in Movie S5).